



Transformations of silicon clathrate Si_{136} under high hydrogen pressure up to 11 GPa

O.I. Barkalov^{*}, M.A. Kuzovnikov, I.A. Sholin, N.S. Orlov

Institute of Solid State Physics Russian Academy of Sciences, Chernogolovka, Moscow District, 2 Academician Ossipyan str., 142432, Russia

ARTICLE INFO

Communicated by Ralph Gebauer

Keywords:

Silicon clathrates
High hydrogen pressure
Raman spectroscopy
ab initio calculations

ABSTRACT

Phase transformations of silicon clathrate Si_{136} under high hydrogen pressure up to 11.5 GPa were studied by *in situ* Raman spectroscopy and X-ray diffraction at room temperature in a diamond anvil cell. The pressure dependencies of the vibrational mode frequencies of Si_{136} agree well with the *ab initio* calculation results. In addition to the “rigid” one-phonon modes a series of “soft” modes was found in the $300 \div 400 \text{ cm}^{-1}$ frequency range, which results from the two-phonon Raman scattering. At the pressure of 10 GPa the silicon clathrate Si_{136} transformed into a mixture of the Si-II (β -Sn-type) and Si-III (BC8-type) phases. During the subsequent decompression down to 9 GPa the Si-II phase transformed to Si-III, which was then recovered to ambient pressure. No interaction between hydrogen and silicon was observed for Si_{136} upon compression and for the Si-II and Si-III phases upon decompression.

1. Introduction

New clathrate allotropes of silicon and germanium were synthesized in 1970 by thermal decomposition of sodium silicide (germanide) NaSi (NaGe) under high vacuum [1]. Two clathrate phases were obtained by this process - sI clathrate $\text{Na}_8\text{Si}_{46}$ and sII clathrate $\text{Na}_x\text{Si}_{136}$ ($0 < x < 24$). It is not possible to remove sodium atoms from the cage-like silicon host structure of the sI phase, because the increase of annealing temperature or prolonged vacuum annealing results in its total decomposition into a stable diamond-like (Si-I) phase of silicon and sodium. In contrast, a prolonged annealing of the sII phase at the moderate temperatures of 380–400 °C allows to reduce the sodium content in the clathrate to $x = 1$. Further treatment of the powder sample by the elemental iodine vapor in the sealed glass tubes produces nearly sodium-free Si_{136} structure [2]. The atomic structure of both phases was thoroughly refined using the Rietveld method for the X-ray diffraction data by Reny et al. in Ref. [3]. The space group of $\text{Na}_x\text{Si}_{136}$ is $Fd\bar{3}m$ with the lattice parameter of $a \approx 14.63 \text{ \AA}$. The cubic unit cell is formed by 16 “small” dodecahedral cages and 8 “large” hexakaidecahedral cages. The sII phase has an expanded structure with the specific volume per silicon atom exceeding that of diamond-like Si by 15%. Resistivity and optical experiments reported in Ref. [4] demonstrated that pure Si_{136} structure has a band gap of 1.9–2.0 eV, which is about twice than that for diamond-like Si-I. The increase of x in the $\text{Na}_x\text{Si}_{136}$ structure results in a gradual

semiconductor-to-metal transition for $x > 8$ [1,5–7]. This effect manifested itself by the weaker Raman signal for $\text{Na}_{10}\text{Si}_{136}$ comparing to that for $\text{Na}_1\text{Si}_{136}$ and $\text{Na}_6\text{Si}_{136}$ [8]. Moreover, the silicon and germanium clathrates $\text{Cs}_8\text{Na}_{16}\text{Si}_{136}$ and $\text{Cs}_8\text{Na}_{16}\text{Ge}_{136}$ with fully occupied cages demonstrated metallic conductivity [9].

The clathrate phase sII is metastable at normal conditions. According to differential calorimetric studies reported in Ref. [10] it transforms irreversibly to the stable diamond-type silicon (Si-I) when heated above $\sim 600 \text{ }^\circ\text{C}$. The compression at room temperature up to 8–10 GPa [11] or 11 GPa [12] results in an irreversible transition of the sII phase into a high pressure Si-II allotrope with the β -tin type structure. According to the *ab initio* predictions the Si_{136} clathrate phase is thermodynamically stable at *negative* pressures of about -3 GPa [13,14].

The sII phase of silicon is isostructural to the inclusion compounds with the host structure formed by H_2O molecules and stabilized by various “guest” atoms or molecules, occupying the cages of the “host” crystalline network [15]. The H_2O clathrate with the sII structure, also called ice XVI [16], can take up sufficient amounts of noble gases or hydrogen [17,18]. However, these materials do not have high thermal stability – at ambient pressure the hydrogen desorption from the quenched sII clathrate hydrate starts at liquid nitrogen temperature and finishes at 220 K by the collapse of the clathrate structure into a mixture of cubic ice I_c and stable hexagonal ice I_h [19]. This fact rules out the extensive technological applications of the clathrate hydrates as

^{*} Corresponding author.

E-mail addresses: barkalov@issp.ac.ru (O.I. Barkalov), kuz@issp.ac.ru (M.A. Kuzovnikov), sholin@issp.ac.ru (I.A. Sholin), orlovns@issp.ac.ru (N.S. Orlov).

<https://doi.org/10.1016/j.ssc.2021.114492>

Received 11 June 2021; Received in revised form 27 July 2021; Accepted 30 July 2021

Available online 29 August 2021

0038-1098/© 2021 Elsevier Ltd. All rights reserved.

hydrogen storage materials. The silicon Si_{136} clathrate is free of that drawback because of its high thermal and mechanical stability. The interaction of the gases with silicon sII clathrate has not been reported so far. In the present work we explored the interaction of hydrogen with silicon framework of the clathrate phase by *in situ* Raman spectroscopy, X-ray diffraction in diamond anvil cell (DAC), and by *ab initio* calculations within the entire stability range of the clathrate phase up to 11 GPa.

2. Methods

The clathrate sample used in the present work was synthesized using the method described elsewhere [1,3,14]. A lump of sodium silicide NaSi was annealed for 22 days under high vacuum conditions ($10^{-6} \div 10^{-9}$ mbar) at the temperature of 400 °C. The resulting material contained 94 wt % $\text{Na}_x\text{Si}_{136}$, 2 wt % $\text{Na}_8\text{Si}_{46}$ and 4 wt % Si-I according to the Rietveld analysis of its X-ray powder diffraction pattern. The total sodium and silicon content in the sample was determined by the energy dispersion X-ray spectroscopy microanalysis system EDS-Oxford Inca Energy 450 in the scanning electron microscope Supra 50VP. The calculated sodium content x of the main clathrate phase $\text{Na}_x\text{Si}_{136}$ was 2.6.

Ultra-low fluorescent diamonds of the modified brilliant cut type with flat culets of about 400 μm in diameter were used in the high-pressure experiment. Rhenium gasket was preindented at pressure of about 12 GPa to about 50 μm thickness, and laser drilling was used to make a hole 200 μm in diameter. Ruby luminescence pressure scale for quasi-hydrostatic condition [20] was used. Ruby lines were sharp and well resolved during all experiment, indicating absence of non-hydrostatic stresses. Pressure determination accuracy was about 0.3 GPa. Ruby fluorescence and Raman spectra were recorded with the THR1000 spectrometer, equipped with a Peltier-cooled CCD detector and a grating of 1200 grooves/mm. The samples were irradiated with a 632.8 nm He-Ne laser line (max laser power ~ 20 mW at sample) at room temperature using a back-scattering geometry. A 20 \times Mitutoyo objective was used to focus the laser beam to a spot of approximately 5 μm in size and collect the scattered light. Tilted holographic SuperNotch-Plus filter from Kaiser Optical Systems allowed spectrum recordings for Raman shifts higher than 90 cm^{-1} .

Hydrogen was loaded into the gasket hole at room temperature and pressure of about 0.3 GPa by the technique described elsewhere [21]. Hydrogen served both as a reagent and as a pressure transmitting medium. Hydrogen was always in excess, and its presence in the cell was monitored both visually and by Raman spectroscopy.

After initial clamping of hydrogen in a DAC the compression force was increased in steps by a lever mechanism. After pressure relaxation of about half an hour the Raman spectra were recorded from several points from the sample surface. Three spectral ranges were recorded for each point: 0-4500 cm^{-1} , 50-890 cm^{-1} and 4080-4310 cm^{-1} . Exposition time for the first range was 100 s per frame, for the last two 500 s per frame. Frames for each spectral range were glued together using standard procedures.

The pressure was measured before and after each X-ray diffraction measurement, and the difference between these values was typically about 1 GPa at pressures of ~ 10 GPa. The pressures referred further are the pressures after the corresponding X-ray or Raman measurements.

X-ray powder diffraction patterns were measured by the energy-dispersive method with a polychromatic radiation from a conventional tungsten target tube and a 100 μm homemade collimator. The X-ray technique is described in more details elsewhere [22]. Each X-ray powder diffraction pattern was collected with an exposition time of ~ 24 h.

The vibrational properties of pure Si_{136} were calculated by a density-functional theory implemented in the CASTEP code [23]. Norm-conserving pseudopotentials with a plane-wave cutoff of 350 eV were used. Calculations were performed under the LDA functional with

exchange and correlation approximation from Ref. [24] as parameterized by Ref. [25]. Brillouin-zone integration was performed according to the Monkhorst-Pack scheme [26] with a $2 \times 2 \times 2$ sampling. Density functional perturbation theory was used to calculate the dynamical matrices [27]. Our calculations at ambient pressure demonstrated that the vibrational frequencies of the Si_{136} were well-converged with respect to the plane-wave cutoff energy and k-point mesh. Particularly, a cutoff increase up to 390 eV in a test calculation shifted each vibrational frequency by less than 0.7 cm^{-1} , which is well below spectroscopic experimental error. Raman intensities were calculated using the method described in Ref. [28].

3. Results and discussion

3.1. X-ray diffraction

The energy-dispersive X-ray powder diffraction spectra, collected upon compression-decompression cycle are shown in the Figure S1 in the Supplementary Materials. During the compression cycle the Si_{136} peaks were observed up to 10 GPa, and then disappeared. At the same pressure a phase transformation of Si_{136} to a β -tin high pressure phase of silicon (Si-II) was reported earlier during Si_{136} compression in an inert medium [11,12]. In our case the peak positions for Si-II substantially overlapped with the rhenium gasket peaks, and could not be resolved. At the same pressure the Raman signal disappeared from nearly whole sample surface (see next section), thus, it was decided to finish the compression at that moment and start decompression.

When decompressed in an inert medium, Si-II transforms into Si-III with a BC8-type structure at about 10 GPa [29]. During the decompression cycle in our experiment only one sample peak could be clearly seen in the diffraction patterns, which is a (211) peak of Si-III. This Si-III is retained at ambient pressure. The Si_{136} and Si-III phases have cubic crystal structures, and their lattice parameters and volumes can be calculated reliably even from low resolution diffraction data. The resulting volumes as a function of hydrogen pressure are shown in Fig. 1 together with available literature data for Si_{136} compression in an inert

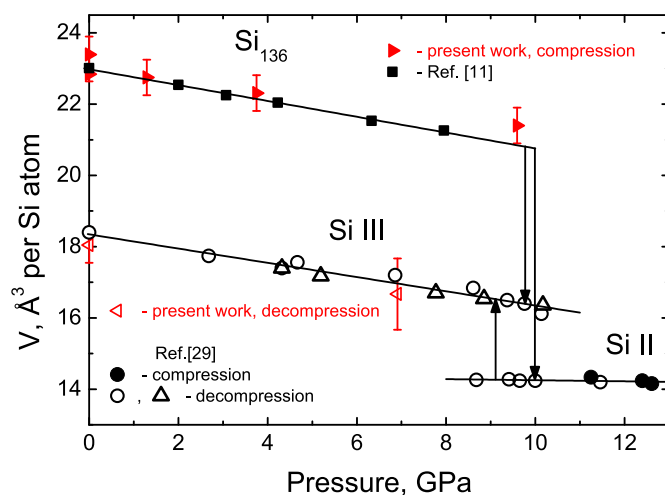


Fig. 1. Atomic volumes of various silicon phases plotted as a function of pressure. The solid and open red triangles show the results of the present work for the compression of the Si_{136} sample and decompression, respectively. The solid squares denote the atomic volume of the silicon clathrate Si_{136} from Ref. [11], the circles and upstanding open triangles stand for the volumes of Si II (β -tin silicon phase) and Si III phases reported in Ref. [29]. In present study, the sample was compressed in a hydrogen atmosphere, whereas a methanol-ethanol mixture was used as a pressure transmitting medium in Refs. [11, 29]. The lines drawn through the data points are the guides for the eye. (For interpretation of the references to color in this figure legend, the reader is referred to the Web version of this article.)

medium.

Our results within the experimental error coincide with the literature data for Si_{136} and Si-III. No volume difference was observed for Si_{136} compressed in hydrogen and in an inert media, in contrast to our previous studies of various metal-hydrogen systems (see e.g. Refs. [30–32], where hydrogen incorporation always resulted in a dramatic volume expansion of solid phase.

It is known that an addition of a new component to a system expands the stability field of a phase with a larger (comparing to the other phases) solubility of this component. Consider, for example, ice-II, which is the stable phase of H_2O at $T < -40^\circ\text{C}$ and $0.2\text{ GPa} < P < 0.6\text{ GPa}$. In a hydrogen atmosphere its stability field is dramatically shifted and expanded up to 2.5 GPa in pressure and 100°C in temperature [33]. This is because the solubility of hydrogen in this phase $\text{H}_2/\text{H}_2\text{O} \sim 1/6$ is much larger than that for the hexagonal ice, liquid water, ice III, ice V and ice VI, which are adjacent phases to ice II in the P-T phase diagram of H_2O . Even more dramatic effect is observed for cubic ice Ic, which does not have any stability field at positive pressures. When hydrogen pressure is applied, this form of ice becomes stable in the pressure range $2\text{ GPa} < P < 30\text{ GPa}$ (at least) because of the high $\text{H}_2/\text{H}_2\text{O} \sim 1$ content in this phase. Similar behavior is observed for the clathrate forms of H_2O , such as ice XVI (sII clathrate hydrate) [17,18].

One would expect similar behavior for Si_{136} , which is structurally isomorphic to ice XVI. If there would be high hydrogen solubility in this phase, then its decomposition conditions should be considerably shifted to higher pressures, because the equilibrium hydrogen solubility in all other silicon phases is zero.

We did not observe any change in the pressure of the Si_{136} to Si-II transformation when hydrogen was used instead of inert pressure transmitting medium. Thus, despite the X-ray scattering by the hydrogen atoms is negligible, we firmly established the absence of any hydrogen solubility in Si_{136} from the absence of any hydrogen-induced side effects.

3.2. Raman spectroscopy

The Raman spectrum of the initial sample was measured at ambient conditions in air (black curve in Fig. 2). It was necessary to decrease the laser power to $\sim 2\text{ mW}$, otherwise new unidentified peaks developed in the spectrum, indicating thermally induced structural decomposition of Si_{136} . At full laser power ($\sim 20\text{ mW}$) the sample converted to pure diamond-like silicon (Si-I).

After loading the sample in the DAC with H_2 the spectral profiles no longer showed any dependence on applied laser power, which is a result of high thermal conductivity of hydrogen and diamond. From that moment full laser power was applied. The Raman spectra were measured at several points on the sample surface at each pressure, and, particularly, one spectrum was always measured at the point above pure hydrogen to compare its spectrum with that for the sample.

Apart from the Raman signal from the Si_{136} phase, the following extra features were present in the spectra – a peak from the Si-I impurity, the rotons and a vibron from H_2 , and a Ne plasma line. The weak peak from the silicon Si-I (diamond-like) impurity phase was located at the Raman shift range of $520\text{--}550\text{ cm}^{-1}$. The sharp Ne plasma line was located at about 133 cm^{-1} , close to the literature value of 136.1 cm^{-1} (6328.99 \AA) [34], and was independent of pressure. Two H_2 roton bands were observed at $300\text{--}400$ and $550\text{--}650\text{ cm}^{-1}$. These bands were shifted and strongly broadened with pressure increase. The peak from the H_2 vibron was observed at about 4200 cm^{-1} , and this peak was shifted and sharpened with pressure increase. The representative spectra of the silicon clathrate sample are shown for the compression and decompression runs in Figs. 2 and 3, respectively.

At the wavenumbers higher than the diamond Raman line at 1330 cm^{-1} the spectra measured during compression and decompression above the sample and above pure H_2 were identical. Particularly, no peaks were observed in any measured spectrum in the interval of $2100\text{--}2400\text{ cm}^{-1}$, which is the characteristic range of a covalent Si-H

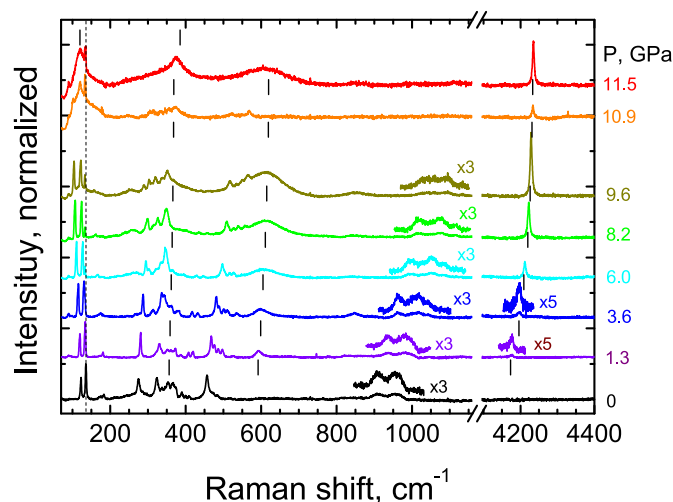


Fig. 2. Raman spectra of the silicon clathrate sample measured in the course of increasing pressure. The broad and featureless background caused by the fluorescence from the sample and diamond anvils was subtracted manually from each spectrum. The intensity was normalized by the amplitude of the $1E_g$ mode peak of the Si_{136} clathrate (133 cm^{-1} at zero pressure). The black ticks below each spectrum denote the frequencies of hydrogen rotons and vibron modes, obtained by the linear fit of the data reported in Ref. [35] for pure hydrogen. The black ticks above the spectrum at 11.5 GPa denote the positions of the Raman peaks from Si-II (β -tin silicon phase) determined by the fit of the data reported in Ref. [36]. The vertical dashed line denotes the position of the He-Ne laser plasma line. The broad and weak peaks due to multiphonon scattering at $\sim 1000\text{ cm}^{-1}$ and hydrogen vibron at $\sim 4200\text{ cm}^{-1}$ are given in enlarged intensity scale above the original spectra. (For interpretation of the references to color in this figure legend, the reader is referred to the Web version of this article.)

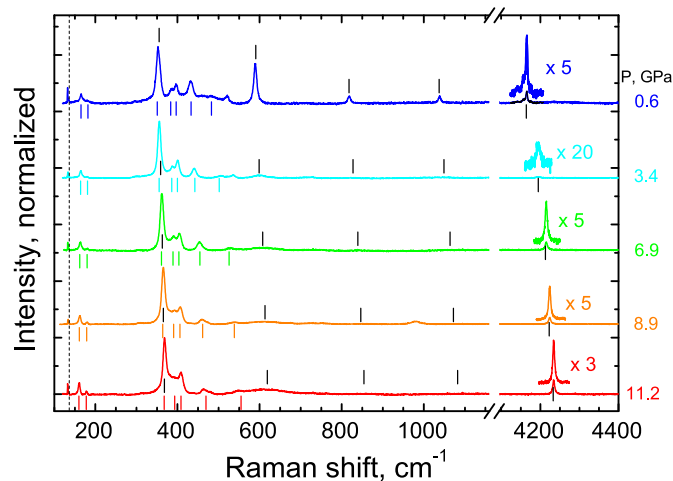


Fig. 3. Raman spectra of silicon sample measured in the course of decreasing pressure. The broad and featureless background caused by the fluorescence from the sample and diamond anvils was subtracted manually from each spectrum. The intensity was normalized by the amplitude of the A_g mode peak of the Si III phase (351 cm^{-1} at 0.6 GPa). The black ticks above and below each spectrum denote the frequencies of hydrogen rotons and vibron modes, obtained by the linear fit of the data reported for pure hydrogen [35]. The other ticks below each spectrum denote the positions of the Raman active modes of the Si-III phase, obtained by the linear fit of the data presented in Ref. [37]. The peak from hydrogen vibron is given in enlarged intensity scale above the original spectra. (For interpretation of the references to color in this figure legend, the reader is referred to the Web version of this article.)

bond stretching. Presence of a silane SiH_4 would unavoidably result in a presence of such peaks [38].

With one exception, all peaks observed in the $600\text{--}1330\text{ cm}^{-1}$ range were assigned either to the H_2 rotors or to the two-phonon Raman scattering from Si_{136} . We observed one unidentified peak at $\sim 980\text{ cm}^{-1}$ at one sample point at 8.9 GPa during decompression (orange curve in Fig. 3). In principle the bending modes of a covalent Si–H bond can be expected at this wavenumber, but the absence of a stretching band in the spectrum, which should be ~ 20 times stronger in intensity, dismisses such interpretation. The peak at $\sim 980\text{ cm}^{-1}$ was not observed in other spectra.

During the compression a considerable Raman signal decrease was observed at 9.6 GPa and above. The sample became inhomogeneous at these pressures, and new peaks developed at few sample points. These peaks, assigned to the Si-III phase, persisted during the rest of the experiment, and, particularly, they were observed at each point on the sample surface during subsequent decompression. At 10.9 GPa and above the peaks from Si_{136} disappeared completely, and virtually no useful signal, except for the Si-III peaks discussed above, can be seen from most sample surface. The broad features at 120 and 380 cm^{-1} , observed in the orange and red spectra in Fig. 2, are characteristic of Si-II [36].

During decompression the sample transformed to Si-III and became homogenous again. The decompression spectra are presented in Fig. 3, and all major peaks in these spectra can be assigned to Si-III [37] and H_2 . In addition, a weak Si–I peak can be seen in the 0.6 GPa spectrum at 520 cm^{-1} (blue curve in Fig. 3). Similar evolution of Raman spectrum upon decompression was reported in Ref. [39]. Note that the authors of this reference incorrectly interpreted the two-phase state $\text{Si}_{136}+\text{Si-III}$ at 9.7 GPa as a new unidentified phase.

The spectral region of the H_2 vibron is presented in Fig. 4 in more details. The positions of the H_2 vibron peak observed on the sample surface and in the pure H_2 phase are shown in Fig. 5 as a function of pressure by triangles and circles, respectively. The literature data for pure H_2 phase from Ref. [35] is shown by the red curves in Fig. 5.

Previously, a considerable shift and a splitting of H_2 vibron were reported for molecular hydrogen filling the clathrate structures. Particularly, for ice XVI filled with H_2 (hydrogen hydrate sII) a system of peaks is observed with shifts ranging from -40 to -5 cm^{-1} , counted from the vibron position in the pure hydrogen phase [18,40,41]. In

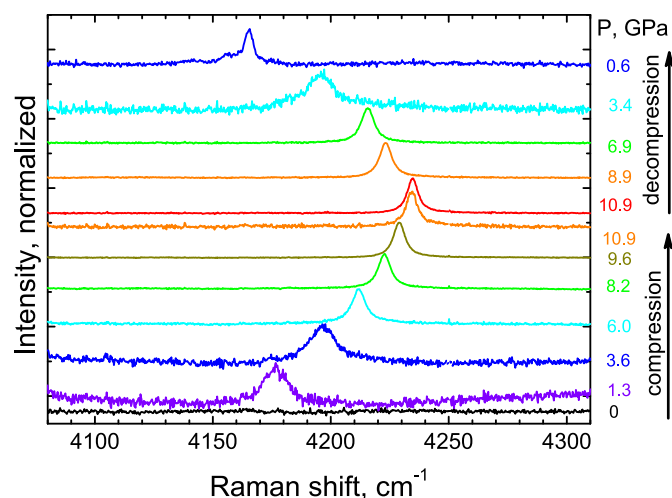


Fig. 4. Raman spectra in the frequency region of hydrogen molecule vibron observed from the surface of the silicon sample in the course of increasing and decreasing pressure. A linear background was manually subtracted from each spectrum, and each spectrum was normalized by the peak intensity. The spectrum at 0 GPa was measured from the sample before loading hydrogen. (For interpretation of the references to color in this figure legend, the reader is referred to the Web version of this article.)

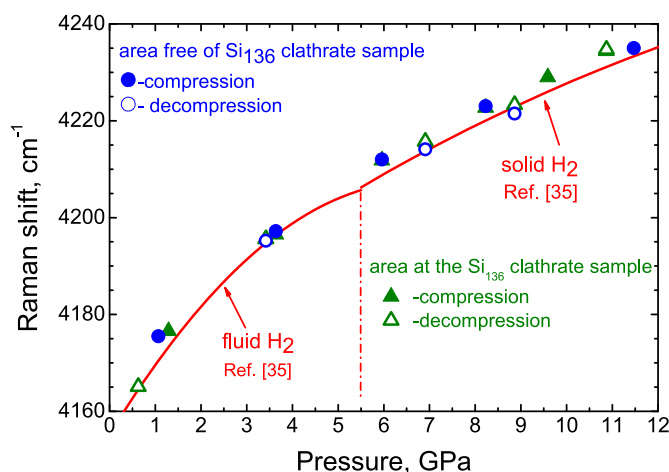


Fig. 5. The position of the hydrogen $Q_1(1)$ vibrational mode plotted as a function of pressure. The solid and open symbols correspond to the compression and decompression, respectively. The circles represent the data obtained from the area in the gasket hole free from the clathrate sample, while the triangles represent the data obtained directly above the Si_{136} sample. The solid lines are polynomial least-square fits for pure hydrogen reported in Ref. [35]. The crystallization of fluid H_2 at 5.5 GPa is shown by the dash-dotted line.

Ref. [18] these peaks were assigned to H_2 molecules occupying large and small cages respectively. Because the cages in the Si_{136} clathrate are smaller by 14% than that for the sII clathrate hydrate, one should expect stronger perturbation of the H_2 vibron by the host crystal field of Si_{136} .

In other hydrogen-filled ices - ice XVII (C0 phase), ice II (C1) and ice Ic (C2) - the vibron splitting is not observed because H_2 molecules occupy only one crystallographic site [40]. The vibron shift, however, is observed for all of the hydrogen-filled clathrate ices. This shift can be positive, e.g. for the C2 hydrate it is about $+30\text{ cm}^{-1}$ [40], or negative, like in the sII hydrate discussed above.

In the present work, no shift and no splitting of the H_2 vibron were observed on the surface of the Si_{136} sample (olive triangles in Fig. 5) comparing to the H_2 vibron in pure hydrogen phase (blue circles in Fig. 5) within experimental accuracy. The absence of H_2 vibron shift and splitting suggests the absence of hydrogen interaction with the silicon sample, which most likely indicates zero hydrogen solubility in it.

Another indication of the absence of hydrogen interaction with the silicon sample comes from the analysis of the pressure evolution of the host Si_{136} lattice modes, discussed in the next section.

3.3. Ab-initio calculations

Standard factor-group analysis shows the following phonon modes at the Γ -point of the Brillouin zone of Si_{136} :

$$\Gamma = (T_{1u})_{\text{acoustic}} + (7T_{1u})_{\text{IR}} + (3A_{1g} + 4E_g + 8T_{2g})_{\text{Raman}} + (A_{1u} + A_{2g} + 3A_{2u} + 4E_u + 5T_{1g} + 5T_{2u})_{\text{silent}}$$

The E modes are doubly degenerate, and the T modes are triply degenerate. Thus, there should be 15 peaks in the Raman spectrum of Si_{136} . The crystal structure has an inversion center, thus, each mode has definite parity (either even “g” or odd “u”) with respect to this inversion center, and could be either Raman active, IR active, or silent. The comparison of the present calculations, the calculations of [42], and presently observed peak positions at normal pressure is presented in Table 1.

The difference between the peak positions in our calculations and that of [42] typically does not exceed $2\text{--}3\text{ cm}^{-1}$. A comparison of the calculated and experimental Raman spectra at 0 GPa is shown in Fig. 6.

The pressure dependencies of the experimental and calculated peak positions are presented in Fig. 7 by the symbols and solid curves,

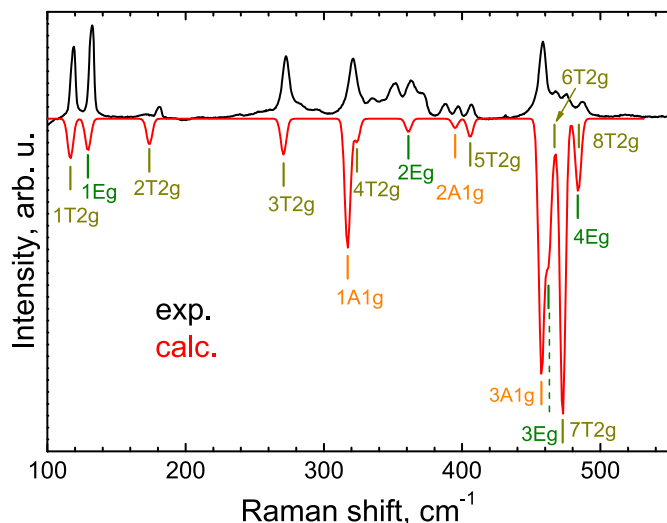


Fig. 6. Experimental (black) and calculated (red) Raman spectra of the silicon clathrate Si_{136} at normal pressure. The ticks with labels show the calculated mode frequencies (see Table 1). (For interpretation of the references to color in this figure legend, the reader is referred to the Web version of this article.)

respectively. Four frequency ranges should be considered separately to make peak assignment. Below 200 cm^{-1} the assignment is obvious (see Table 1 and Fig. 6). In the $250\text{--}450\text{ cm}^{-1}$ range there are 8 peaks in the 0 GPa spectrum but 6 in the calculations. In the $450\text{--}500\text{ cm}^{-1}$ range there are 6 modes with closely spaced frequencies in our calculations but only 4 peaks in the experimental spectrum (Fig. 6), thus, the assignment for this region can be arbitrary. The positions of the peaks at $900\text{--}1100\text{ cm}^{-1}$ are in a good agreement with the doubled calculated frequencies of the maxima at the phonon densities of states, thus indicating the two-phonon origin of these peaks.

In the $300\text{--}400\text{ cm}^{-1}$ interval six peaks were observed at ambient pressure, whereas only four peaks were predicted by calculations (see Table 1). Previously, only three peaks were observed in this range at 325 , 360 and 387 cm^{-1} in Ref. [14], whose frequencies decreased with pressure increase. These peaks were incorrectly assigned to the first-order Raman scattering by the T_{2g} , E_g and A_{1g} clathrate modes despite the prediction of the positive Grueneisen parameters for these modes [14]. Presently, we assign the soft modes, observed at 335 , 352 and 388 cm^{-1} at 0 GPa (open red circles in Fig. 7) to the two-phonon processes involving the soft modes of Si_{136} below 200 cm^{-1} (Fig. 7).

Taking this into account, the rest of the peaks can be easily assigned to the Si_{136} modes (see Table 1). There is a good overall agreement between our experiment and calculations. The difference of the calculated mode frequencies and corresponding experimental peak positions does not exceed 10 cm^{-1} at all pressures. No anomalies, such as nonlinearity or discontinuities, can be seen in the pressure evolution of the experimental peak positions and the pressure dependencies of all modes are well explained by the calculations for pure Si_{136} . Thus, the effect of hydrogen on the host Si_{136} lattice modes is negligible.

To elaborate the effect of H_2 incorporation into the Si_{136} structure, we performed *ab initio* calculations for the hypothetical $\text{Si}_{136}(\text{H}_2)_8$ structure, in which one hydrogen molecule is placed into each large cage of the host Si_{136} lattice. The calculated value of the enthalpy H for the reaction $\text{Si}_{136} + 8\text{H}_2 = \text{Si}_{136}(\text{H}_2)_8$ is $H = -1.65\text{ eV}$ per H_2 molecule at 10 GPa and 0 K, which seems to favor such incorporation. This result should, however, be taken with caution, because presently available *ab initio* calculation methods dramatically underestimate the enthalpies of hydrides.

Our calculations predict only a minor effect of hydrogen incorporation on the volume and vibrational properties of the host Si_{136} structure. Particularly, the shift of the vibrational frequency is from -1 to $+3\text{ cm}^{-1}$

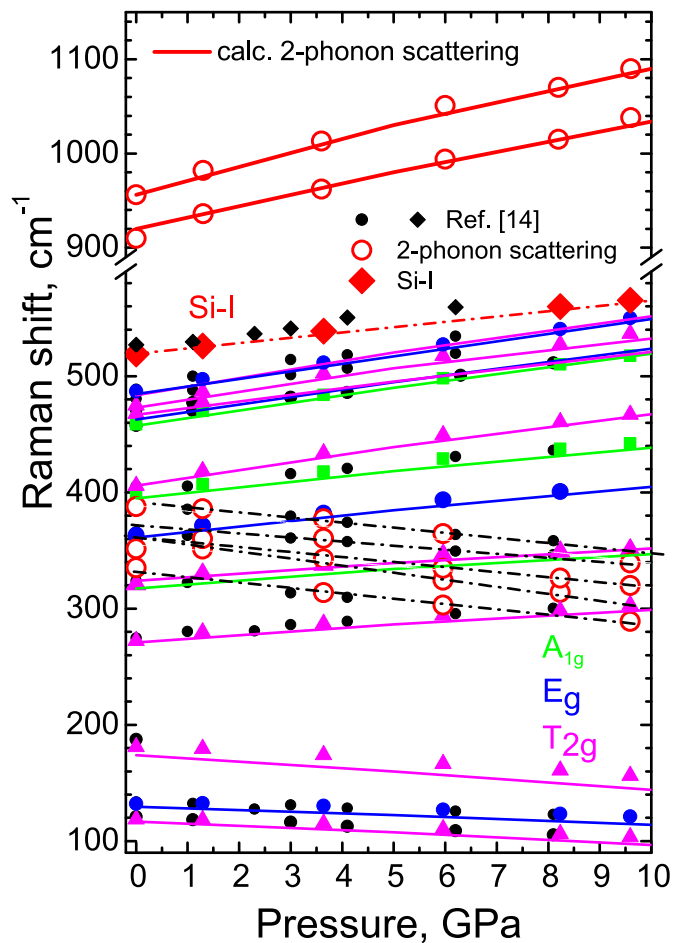


Fig. 7. Frequencies of the Raman active modes of the silicon clathrate Si_{136} sample plotted as a function of pressure. The black symbols denote the experimental peak positions from Ref. [14], the symbols of other colors stand for the experimental data of the present work, and the solid lines are the results of present calculation. The solid red lines in the high frequency region (above 900 cm^{-1}) represent the calculation results of the present work for two-phonon modes. The open red circles denote the experimental positions of two-phonon peaks from the Si_{136} clathrate. The black dash and dot lines drawn through the data points are the guides for the eye, which show the pressure evolution of the “soft” modes, originating from two-phonon scattering. The red and black diamonds represent the Raman peak position of the impurity phase of the diamond-type silicon Si-I from the present work and from Ref. [14], respectively. The peak positions at ambient pressure are listed in Table 1. (For interpretation of the references to color in this figure legend, the reader is referred to the Web version of this article.)

for each Raman-active mode. On the other hand, the changes of the vibrational properties of H_2 upon entering the Si_{136} structure are dramatic – the vibron frequency shift by about $+200\text{ cm}^{-1}$. Presumably, in the small cage the shift should be even stronger because of stronger interaction between the H_2 and its environment. The absence of any peaks which can be associated with the shifted vibron in experiment (see Section 3.2) indicates the absence of hydrogen in our silicon sample.

4. Conclusions

We studied the behavior of silicon clathrate Si_{136} under high hydrogen pressure up to 11.5 GPa by X-ray powder diffraction and Raman spectroscopy at room temperature. During compression, silicon clathrate irreversibly transformed into a mixture of Si-II and Si-III at about 10 GPa . During decompression Si-II transformed into Si-III at about 9 GPa .

Table 1

Calculated and experimental Raman frequencies for the silicon clathrate Si₁₃₆ at ambient pressure.

| Mode | Wavenumber, cm ⁻¹ | | |
|------------------|------------------------------|------------------|----------------------------------|
| | Calculation, present work | Calculation [42] | Experiment, present work |
| 1T _{2g} | 117 | 121 | 119 |
| 1E _g | 129 | 128 | 133 |
| 2T _{2g} | 174 | 176 | 181 |
| 3T _{2g} | 271 | 267 | 272 |
| 1A _{1g} | 317 | 316 | 321 |
| 4T _{2g} | 324 | 325 | unresolved from 1A _{1g} |
| two-phonon | – | – | 335 |
| two-phonon | – | – | 352 |
| 2E _g | 361 | 360 | 363 |
| two-phonon | – | – | 388 |
| 2A _{1g} | 395 | 397 | 397 |
| 5T _{2g} | 406 | 406 | 407 |
| 3A _{1g} | 457 | 458 | 459 |
| 3E _g | 463 | 463 | 468 |
| 6T _{2g} | 467 | 466 | unresolved from 3E _g |
| 7T _{2g} | 473 | 473 | 475 |
| 4E _g | 484 | 483 | 487 |
| 8T _{2g} | 484 | 487 | unresolved from 4E _g |

No indications of the interaction of molecular hydrogen with the host lattice of the silicon clathrate Si₁₃₆ were observed within the pressure range covered in our experiments. Thus, the H₂ molecules did not penetrate into the cages of the Si₁₃₆ crystal structure. In addition, we did not observe hydrogen absorption by the Si-II and Si-III phases. Our experimental pressure dependencies of the Si₁₃₆ Raman mode frequencies are in a good agreement with the data reported in Ref. [14] for Si₁₃₆ compressed in an inert medium. Our *ab initio* calculations describe the observed pressure dependencies of peak positions with satisfactory accuracy, which allowed us to unambiguously assign all observed Raman peaks.

Particularly, three additional “soft” modes, whose frequencies decrease with pressure increase, were found in the 300 ÷ 400 cm⁻¹ frequency range. These “soft” modes were the only ones recorded experimentally in Ref. [14] in this range, and they were incorrectly assigned to the T_{2g}, E_g and A_{1g} modes of the Si₁₃₆ lattice. However, all single-phonon modes in the 300 ÷ 400 cm⁻¹ range should be “rigid” according to the calculations in Ref. [14] and present ones. Therefore, we assign these modes to the two-phonon scattering processes involving the soft modes in the 150 ÷ 200 cm⁻¹ range.

Author statement

O.I. Barkalov: Conceptualization, Methodology, Investigation, Writing. M.A. Kuzovnikov: Methodology, Investigation, Software, Writing. I.A. Sholin: Investigation, Writing, Writing – original draft preparation. N.S. Orlov: Investigation, Writing, Writing – original draft preparation.

Declaration of competing interest

The authors declare that they have no known competing financial interests or personal relationships that could have appeared to influence the work reported in this paper.

Acknowledgments

The authors wish to thank the Institute of Physical Chemistry of Polish Academy of Sciences for offering the high pressure experimental facilities. This work was carried out within the state task of the Institute

of Solid State Physics Russian Academy of Sciences. The financial support of the Program RAS Nr. P11 “Thermal physics of high energy densities. Matter under high pressure” is gratefully acknowledged.

Appendix A. Supplementary data

Supplementary data to this article can be found online at <https://doi.org/10.1016/j.ssc.2021.114492>.

References

- [1] C. Cros, M. Pouchard, P. Hagenmuller, Sur une Nouvelle Famille de Clathrates Minéraux Isotypes des Hydrates de Gaz et de Liquides, *Interprétation des résultats Obtenus* J. Solid State Chem. 2 (1970) 570–581.
- [2] A. Ammar, C. Cros, M. Pouchard, N. Jaussaud, J.-M. Bassat, G. Villeneuve, M. Duttine, M. Ménétrier, E. Reny, On the clathrate form of elemental silicon, Si₁₃₆: preparation and characterization of NaxSi₁₃₆ (x→0), *Solid State Sci.* 6 (2004) 393–400.
- [3] E. Reny, P. Gravereau, C. Cros, M. Pouchard, Structural characterizations of the NaxSi₁₃₆ and Na₈Si₁₄₆ silicon clathrates using the Rietveld method, *J. Mater. Chem.* 8 (1998) 2839–2844.
- [4] J. Gryko, P.F. McMillan, R.F. Marzke, G.K. Ramachandran, D. Patton, S.K. Deb, O. F. Sankey, Low-density framework form of crystalline silicon with a wide optical band gap, *Phys. Rev. B* 62 (2000) R7707–R7710.
- [5] N.F. Mott, Properties of compounds of type NaxSi₁₄₆ and NaxSi₁₃₆, *J. Solid State Chem.* 6 (1973) 348–351.
- [6] A.A. Demkov, O.F. Sankey, K.E. Schmidt, G.B. Adams, M. O’Keeffe, Theoretical investigation of alkali-metal doping in Si clathrates, *Phys. Rev. B* 50 (1994) 17001–17008.
- [7] V.I. Smelyansky, J.S. Tse, The electronic structure of metallo-silicon clathrates NaxSi₁₃₆ (x = 0, 4, 8, 16, 24), *Chem. Phys. Lett.* 264 (1997) 459–465.
- [8] Y. Guyot, B. Champagnon, E. Reny, C. Cros, M. Pouchard, P. Melinon, A. Perez, I. Gregora, Raman scattering of silicon clathrates, *Phys. Rev. B* 57 (1998) R9475–R9477.
- [9] G.S. Nolas, D.G. Vanderveer, A.P. Wilkinson, J.L. Cohn, Temperature dependent structural and transport properties of the type II clathrates A₈Na₁₆E₁₃₆ (A=Cs or Rb and E = Ge or Si), *J. Appl. Phys.* 91 (2002) 8970–8973.
- [10] M. Beekman, G.S. Nolas, Synthesis and thermal conductivity of type II silicon clathrates, *Physica B* 383 (2006) 111–114.
- [11] G.K. Ramachandran, P.F. McMillan, S.K. Deb, M. Somayazulu, J. Gryko, J. Dong, O. F. Sankey, High-pressure phase transformation of the silicon clathrate Si₁₃₆, *J. Phys.: Condens. Matter* 12 (2000) 4013–4020.
- [12] A. San-Miguel, P. Kéghélian, X. Blase, P. Melinon, A. Perez, J.P. Itié, A. Polian, E. Reny, C. Cros, M. Pouchard, High pressure behavior of silicon clathrates: a new class of low compressibility materials, *Phys. Rev. Lett.* 83 (1999) 5290–5293.
- [13] M. Wilson, P.F. McMillan, Crystal-liquid phase relations in silicon at negative pressure, *Phys. Rev. Lett.* 90 (2003) 135703.
- [14] X. Tang, J. Dong, P. Hutchins, O. Shebanova, J. Gryko, P. Barnes, J.K. Cockcroft, M. Vickers, P.F. McMillan, Thermal properties of Si₁₃₆: theoretical and experimental study of the type-II clathrate polymorph of Si, *Phys. Rev. B* 74 (2006), 014109.
- [15] E.D. Sloan, C.A. Koh, *Clathrate Hydrates of Natural Gases*, third ed., CRC Press, Boca Raton London New York, 2008.
- [16] A. Falenty, T.C. Hansen, W.F. Kuhs, Formation and properties of ice XVI obtained by emptying a type sII clathrate hydrate, *Nature* 516 (2014) 231–234.
- [17] A. Dyadin Yu, E.G. Larionov, E. Ya Aladko, A. Yu Manakov, F.V. Zhurko, T. V. Mikina, V. Yu Komarov, E.V. Grachev, Clathrate formation in water-noble gas (hydrogen) systems at high pressures, *J. Struct. Chem.* 40 (1999) 790–795.
- [18] W.L. Mao, H.-K. Mao, A.F. Goncharov, V.V. Struzhkin, Q. Guo, J. Hu, J. Shu, R. J. Hemley, M. Somayazulu, Y. Zhao, Hydrogen clusters in clathrate hydrate, *Science* 297 (2002) 2247–2249.
- [19] V.S. Efimchenko, V.E. Antonov, O.I. Barkalov, A.I. Beskrovnyy, V.K. Fedotov, S. N. Klyamkin, Phase transitions and equilibrium hydrogen content of phases in the water–hydrogen system at pressures to 1.8 kbar, *High Pres. Res.* 26 (2006) 439–443.
- [20] H.K. Mao, J. Xu, P.M. Bell, Calibration of the ruby pressure gauge to 800 kbar under quasi-hydrostatic conditions, *J. Geophys. Res.* 91 (B5) (1986) 4673–4676.
- [21] M. Tkacz, Novel high-pressure technique for loading diamond anvil cell with hydrogen Polish, *J. Chem.* 69 (1995) 1205–1209.
- [22] M. Tkacz, S. Majchrzak, B. Baranowski, High Pressure X-Ray Diffraction Study of Copper Hydride at Room Temperature High Pressure Res, vol. 6, 1990, pp. 85–90.
- [23] S.J. Clark, M.D. Segall, C.J. Pickard, P.J. Hasnip, M.I.J. Probert, K. Refson, M. C. Payne, First principles methods using CASTEP *Z. Kristallografiya* 220 (2005) 567–570.
- [24] D.M. Ceperley, B.J. Alder, Ground state of the electron gas by a stochastic method, *Phys. Rev. Lett.* 45 (1980) 566–569.
- [25] J.P. Perdew, A. Zunger, Self-interaction correction to density-functional approximations for many-electron systems, *Phys. Rev. B* 23 (1981) 5048–5079.
- [26] H.J. Monkhorst, J.D. Pack, Special points for Brillouin-zone integrations, *Phys. Rev. B* 13 (1976) 5188–5192.
- [27] K. Refson, P.R. Tulip, S.J. Clark, Variational density-functional perturbation theory for dielectrics and lattice dynamics, *Phys. Rev. B* 73 (2006) 155114.

- [28] D. Porezag, M.R. Pederson, Infrared intensities and Raman-scattering activities within density-functional theory, *Phys. Rev. B* 54 (1996) 7830–7836.
- [29] J.Z. Hu, I.L. Spain, Phases of Silicon at High Pressure *Solid State Commun.*, vol. 51, 1984, pp. 263–266.
- [30] M.A. Kuzovnikov, M. Tkacz, High pressure studies of cobalt-hydrogen system by x-ray diffraction, *J. Alloys Compd.* 650 (2015) 884–886.
- [31] M.A. Kuzovnikov, M. Tkacz, Synthesis of ruthenium hydride, *Phys. Rev. B* 93 (2016), 064103.
- [32] M.A. Kuzovnikov, H. Meng, M. Tkacz, Nonstoichiometric molybdenum hydride, *J. Alloys Compd.* 694 (2017) 51–54.
- [33] W.L. Vos, L.W. Finger, R.J. Hemley, H. Mao, Novel H₂-H₂O clathrates at high pressures, *Phys. Rev. Lett.* 71 (1993) 3150–3153.
- [34] A.R. Striganov, N.S. Sventitskii, *Tables of Spectral Lines of Neutral and Ionized Atoms*, Plenum, NewYork, 1968.
- [35] S.K. Sharma, H.K. Mao, P.M. Bell, Raman measurements of hydrogen in the pressure range 0.2 - 630 kbar at room temperature, *Phys. Rev. Lett.* 44 (1980) 886–888.
- [36] H. Olijnyk, Raman scattering in metallic Si and Ge up to 50 GPa, *Phys. Rev. Lett.* 68 (1992) 2232–2234.
- [37] M. Hanfland, K. Syassen, Raman Modes of Metastable Phases of Si and Ge *High Pressure Res.*, vol. 3, 1990, pp. 242–244.
- [38] X.-J. Chen, V.V. Struzhkin, Y. Song, A.F. Goncharov, M. Ahart, Z. Liu, H.-K. Mao, R. J. Hemley, Pressure-induced metallization of silane P, *Natl. Acad. Sci. USA* 105 (2008) 20–23.
- [39] P.F. McMillan, O. Shebanova, D. Daisenberger, R.Q. Cabrera, E. Bailey, A. Hector, V. Lees, D. Machon, A. Sella, M. Wilson, Metastable phase transitions and structural transformations in solid-state materials at high pressure, *Phase Transit.* 80 (10–12) (2007) 1003–1032.
- [40] T.A. Strobel, M. Somayazulu, S.V. Sinogeikin, P. Dera, R.J. Hemley, Hydrogen-stuffed, quartz-like water ice, *J. Am. Chem. Soc.* 138 (2016) 13786–13789.
- [41] L. del Rosso, M. Celli, L. Ulivi, New porous water ice metastable at atmospheric pressure obtained by emptying a hydrogen-filled ice, *Nat. Commun.* 7 (2016) 13394.
- [42] J. Dong, O.F. Sankey, G. Kern, Theoretical study of the vibrational modes and their pressure dependence in the pure clathrate-II silicon framework, *Phys. Rev. B* 60 (1999) 950–958.